Research Square

Preprints are preliminary reports that have not undergone peer review.
They should not be considered conclusive, used to inform clinical practice,
or referenced by the media as validated information.

Effect of Nb2O5-TiO2 Co-doping on the Properties of ITO Targets

Yuwen Pang
Guilin University of Electronic Technology
Yi Zhong
Guilin University of Electronic Technology
Guisheng Zhu
zhuguisheng@guet.edu.cn

Guilin University of Electronic Technology
Shenfeng Long
Guilin University of Electronic Technology
Xupeng Jiang
Guilin University of Electronic Technology
Huarui Xu
Guilin University of Electronic Technology

Research Article

Keywords: Nb2O5-TiO2 co-doping, ITO target, Resistivity, Relative density, Carrier mobility

Posted Date: November 16th, 2026

DOI: https://doi.org/10.21203/rs.3.rs-11533697/v1

License: This work is licensed under a Creative Commons Attribution 4.0 International License.
Read Full License

Additional Declarations: No competing interests reported.

Effect of Nb_2O_5-TiO_2 Co-doping on the Properties of ITO Targets

Yuwen Pang[1], Yi Zhong[1], Guisheng Zhu[1,*], Shenfeng Long[1], Xupeng Jiang[1], Huarui Xu[1]

(1. School of Materials Science and Engineering, Guilin University of Electronic Technology; Engineering Research Center of Electronic Information Materials and Devices, Ministry of Education; Guangxi Key Laboratory of Information Materials, Guilin 541004, Guangxi, China)

Abstract With the development of high-performance high-end display devices and the iterative upgrading of photovoltaic cells, higher requirements have been imposed on ITO targets. The preparation technology for ITO targets with high carrier mobility has therefore become a research focus in related fields. Conventional ITO targets have relatively low carrier mobility (30–40 $cm^2 \cdot V^{-1} \cdot s^{-1}$), making it difficult to meet the performance requirements of transparent conductive oxide targets for the next generation of high-end displays and photovoltaic devices. In this study, 0.1 wt% Nb_2O_5 and 0.1 wt% TiO_2 were co-doped into an indium tin oxide powder (In_2O_3:SnO_2 = 9:1, wt%). After die pressing and cold isostatic pressing, ITO green bodies were prepared and sintered in an oxygen atmosphere at 1450 °C for 6 h, yielding an ITO target with a relative density of 99.54%, a resistivity of 1.940×10^{-4} Ω·cm, and a carrier mobility of 57.4 $cm^2 \cdot V^{-1} \cdot s^{-1}$. The results showed that an appropriate amount of Nb_2O_5-TiO_2 co-doping could improve the carrier mobility of ITO targets. In addition, Nb_2O_5-TiO_2 co-doping could reduce the sintering temperature of the ITO target from 1550 °C to 1450 °C. This study achieved the preparation of an ITO target with high density and high mobility while reducing the sintering temperature, providing a reference for the development of low-temperature sintering processes for high-performance ITO transparent conductive targets and for research on TCO materials for high-end displays and photovoltaic devices.

* **Corresponding author** Guisheng Zhu,E-mail zhuguisheng@guet.edu,cn

About the first author Yuwen Pang（2000-）,male,Master candidate,supervised by Professor Guisheng Zhu,research is focused on the performance study of ITO targets.

Key word Nb_2O_5-TiO_2 co-doping; ITO target; Resistivity; Relative density; Carrier mobility

1 Introduction

Transparent conductive oxides (TCOs), featuring excellent visible-light transmittance and electrical conductivity, serve as the core raw materials for magnetron-sputtered thin films applied in flat-panel displays[1], photovoltaic cells[2] and flexible optoelectronic devices. At present, indium-based materials remain the mainstream TCO materials in industry, attracting extensive attention and research owing to their excellent comprehensive performance. Among indium-based targets, ITO features the most mature manufacturing process, optimal balanced optoelectronic properties and the largest commercial-scale consumption when compared with IGZO[3], IWO[4] and IZO[5]. In recent years, the booming development of high-end electronic products and photovoltaic cells has driven a continuous growth in the demand for ITO targets and thin films, while imposing increasingly stringent requirements on their [6]performance[6].In the field of organic light[7]-emitting diodes (OLEDs)[8-10], conventional ITO suffers from excessively low carrier mobility, which readily gives rise to non-uniform high-resolution display in OLED panels[11]. Meanwhile, it increases power consumption, reduces the probability of carrier injection into organic layers, accelerates the degradation of organic materials, and raises the risk of leakage current[12]. By contrast, high-mobility ITO[13] can mitigate the issues of low driving voltage and uneven luminance and enhance the efficiency of carrier injection into organic layers[14]. As a result, OLED displays are capable of delivering images with high contrast and vivid colors. Since high-mobility ITO can satisfy the current development requirements of OLED displays, investigating such materials has become a critical route to break through the performance bottlenecks of high-refresh-rate panels. Improvement in the carrier mobility of ITO thin-film has been regarded as a key research priority. To obtain ITO thin-films with high carrier mobility, research emphasis has gradually shifted to the carrier mobility of ITO targets themselves. Doping modification[15] is recognized as an effective approach for improving the carrier mobility of ITO targets. Ce, Bi, Zn, V, Zr and other elements are commonly adopted as doping elements. As can be seen from Table 1, in early-stage investigations, several doping elements such as Bi and V were found by Muraoka M et al.[16-18] to lower the sintering temperature of ITO targets. Nevertheless, due to the immature sintering technologies, ITO targets with low relative density and high resistivity were obtained. With the advancement of research, doping elements including Zn and Ce were reported by Chen D et al and Huang J et al[19, 20]. to enable the fabrication of ITO targets with high density and low resistivity below 1500 °C when combined with well-established sintering processes. Meanwhile, through studies on binary doping conducted by Liang F et al,Zhai X et al and Liu T et al.[21-23],binary dopants were verified to appropriately supply extra free electrons for tuning carrier concentration while modifying crystal structures and optimizing micro-morphologies. Not only was the sintering temperature reduced, but the resistivity was also substantially decreased. In addition, remarkable influences on the mobility of

ITO targets are exerted by dopants. In 2017, Fei Liang et al. investigated the effect of Bi_2O_3-Nb_2O_5 binary doping on ITO targets and proved that the carrier mobility was effectively enhanced. In 2026, according to the research outcomes presented by Chenguang Ge et al.[24], the carrier mobility of Zr-doped indium-oxide-based targets could be elevated by Ge-Ti co-doping, and novel insights were thereby provided for the mobility improvement of indium-oxide-based ceramic targets. The effects exerted by doping on indium-oxide-based targets demonstrate that doping modification can be utilized as an effective strategy to optimize the comprehensive performances and boost the carrier mobility of targets. However, systematic investigations are still lacking concerning the synergistic effects of the Nb_2O_5-TiO_2 co-doping system on the density, resistivity and carrier mobility of ITO targets.

Table 1 Comparison of properties of ITO targets doped with different dopants

Author	Dopant	Temperature	Resistivity	Relative density
Muraoka M[15]	Bi_2O_3	1500℃	$8.100\times10^{-4}\Omega\cdot cm$	95.00%
Suzuki M[16]	V_2O_5	1400℃	$5.500\times10^{-4}\Omega\cdot cm$	96.00%
Chen D[17]	ZnO	1358℃	$2.000\times10^{-4}\Omega\cdot cm$	98.10%
Jingwei Huang[18]	CeO_2	1500℃	$1.870\times10^{-4}\Omega\cdot cm$	99.60%
Fei Liang[19]	Bi_2O_3-Nb_2O_5	1450℃	$1.780\times10^{-4}\Omega\cdot cm$	99.60%
Xiaoyu Zhai[20]	Bi_2O_3-TiO_2	1550℃	$3.050\times10^{-4}\Omega\cdot cm$	98.70%
Ting Liu[21]	Bi_2O_3-CeO_2	1500℃	$1.820\times10^{-4}\Omega\cdot cm$	99.57%

In the present work, the Nb_2O_5-TiO_2 co-doping method is adopted to investigate its influences on the properties of ITO targets (In_2O_3 wt%: SnO_2 wt% = 9:1). It has been revealed in previous studies that TiO_2 can be used as a sintering aid, by which the sintering temperature of ITO targets is lowered and target densification is promoted; meanwhile, abnormal grain growth is suppressed[25]. Improvements in the carrier mobility of ITO are expected to be achieved by TiO_2 doping[26]. When an appropriate amount of Nb_2O_5 is incorporated, extra electrons are provided by high-valence-state Nb^{5+} and Ti^{4+} ions, the carrier concentration is tuned, and the defect structure is altered, whereby significant effects are imposed on carrier mobility. In this paper, the TiO_2 doping content is fixed at 0.1 wt%, and the effects of varying Nb_2O_5 doping contents as well as different sintering temperatures under identical doping content on the microstructure, relative density, resistivity and carrier mobility of ITO targets are

studied. It is demonstrated by the experimental results that for the ITO target co-doped with 0.1 wt% Nb_2O_5–0.1 wt% TiO_2, a resistivity of 1.94×10^{-4} Ω·cm, a relative density of 99.54%, and a carrier mobility of 57.4 $cm^2\cdot V^{-1}\cdot s^{-1}$ are obtained after heating up to 1450 °C at a heating rate of 2 °C/min and holding for 6 h.

2 Experimental

2.1 Sample preparation

Nanocrystalline In_2O_3, SnO_2, TiO_2 and Nb_2O_5 powders(The information of experimental powders is shown in Table 3) were mixed in accordance with the proportions given in Table 2 and loaded into individual ball-milling jars. Absolute ethanol was employed as the dispersant with a mass ratio of 3:1 relative to the mixed powders, and the total mass ratio of zirconia balls to mixed powders was adjusted to 2:1. The ball-milling jars charged with raw materials were mounted on a planetary ball mill, where the rotational speed was fixed at 350 r/min and the milling process was carried out for 6 h[27]. The resulting mixed slurry was dried, and then passed through a 150-mesh sieve. A 5 wt% polyvinyl alcohol (PVA) solution was incorporated for granulation, and the granulated powders were sieved again to obtain the final ITO powders for forming. ITO powders with different doping ratios were dry-pressed using a die press at 10 MPa with a holding time of 3 min. Subsequent cold isostatic pressing (CIP) was performed at 200 MPa for 10 min, and ITO green bodies of various doping compositions were thereby prepared. These ITO green bodies were placed into a high-temperature tube furnace, dewaxed at 600 °C for 3 h in air, and then sintered at different temperatures (1400 °C, 1450 °C, 1500 °C, 1550 °C, 1600 °C) under pure oxygen atmosphere(99.99%). Sintering was conducted withan oxygen flow rate of 2 L/min, and the holding time at each target temperature was 6 h.

Table 2 Compositions of the differently doped ITO targets (wt%)

wt%	In_2O_3	SnO_2	TiO_2	Nb_2O_5
ITO-0	90.000%	10.000%	0	0
ITO-1	89.892%	9.988%	0.1%	0.02%
ITO-2	89.865%	9.985%	0.1%	0.05%
ITO-3	89.820%	9.980%	0.1%	0.1%
ITO-4	89.640%	9.960%	0.1%	0.3%

Table 3 Information of experimental powders

powder	purity	supplier
In_2O_3	AR	Crystal Union Photoelectric Materials
SnO_2	AR	Crystal Union Photoelectric Materials
TiO_2	99.99%	Aladdin
Nb_2O_5	99.98%	Aladdin

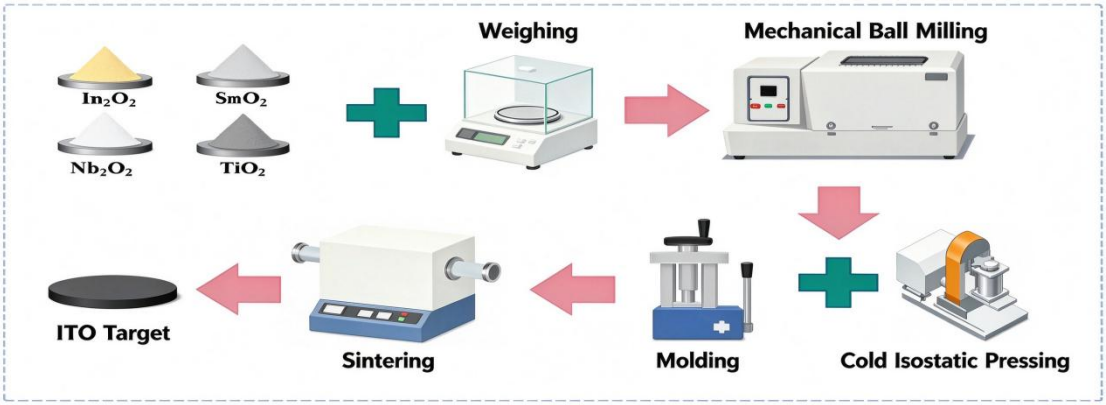


Fig. 1 Process flow diagram of ITO target fabrication

2.2 Characterization

In the present work, the relative density, phase composition, phase structure, resistivity and carrier mobility of ITO targets are mainly analyzed and discussed. The actual density of the ITO targets is measured by the Archimedes method. The relative density is calculated by comparing the measured actual density with the theoretical density of the ITO target (7.15 g/cm³). The specific formula is expressed as follows:

$$\rho_3 = \frac{\rho_1 m_1}{\rho_2 (m_2 - m_3)} \quad (1)$$

In Equation (1), ρ_1 denotes the density of the immersion solution (deionized water was selected as the immersion solution in this experiment, with a density of 1 g/cm^3); ρ_2 represents the theoretical density (7.15 g/cm^3) of the ITO target (In_2O_3 wt%: SnO2 wt% = 9:1);ρ_3 is the relative density of the target; m_1 is the dry mass of the target; m_2 is the saturated wet mass of the target; and m_3 stands for the suspended mass of the target.

Phase compositions of the targets were analyzed by an X-ray diffractometer (XRD, D8-ADVANCEA, Bruker). The microstructures of the ITO targets were characterized using a Schottky field-emission scanning electron microscope (JSM-7610F Plus), and the elemental distributions of the targets were examined by the equipped energy-dispersive X-ray spectroscopy (EDS). The carrier mobility and resistivity of the targets were measured by a Hall-effect measurement system (Lake Shore 8404, Lake Shore Cryotronics, USA) based on the Van der Pauw method.

3 Results and discussion

Figure 2 shows the X-ray diffraction patterns of ITO targets with various Nb_2O_5 doping contents (TiO_2 content fixed at 0.1 wt%), which were sintered at 1450 °C for 6 h with a heating rate of 2 °C/min. Only single-phase ITO diffraction peaks were detected for all ITO targets with different doping levels, and no impurity peaks were observed in the XRD patterns. From the magnified view of the (222) diffraction peak, a right-shift of peak positions can be identified for the doped ITO targets compared with the undoped sample, indicating lattice contraction after doping[28]. This demonstrates

that dopant elements have been incorporated into the ITO lattice to form solid solutions. XRD patterns of ITO targets with different doping concentrations were analyzed, and their lattice constants are summarized in Table 3. Slightly reduced lattice constants were obtained for doped ITO targets relative to the undoped counterpart, which further confirms that the incorporation of dopant elements induces lattice distortion within the ITO lattice. The fact that the lattice constant does not exhibit a decreasing trend with increasing doping concentration may be attributed to the concurrent variation of oxygen-vacancy defects[29]. Higher diffraction-peak intensities were recorded for the doped ITO targets, revealing that appropriate doping can improve the crystallization quality and enhance the crystallographic integrity of ITO targets.

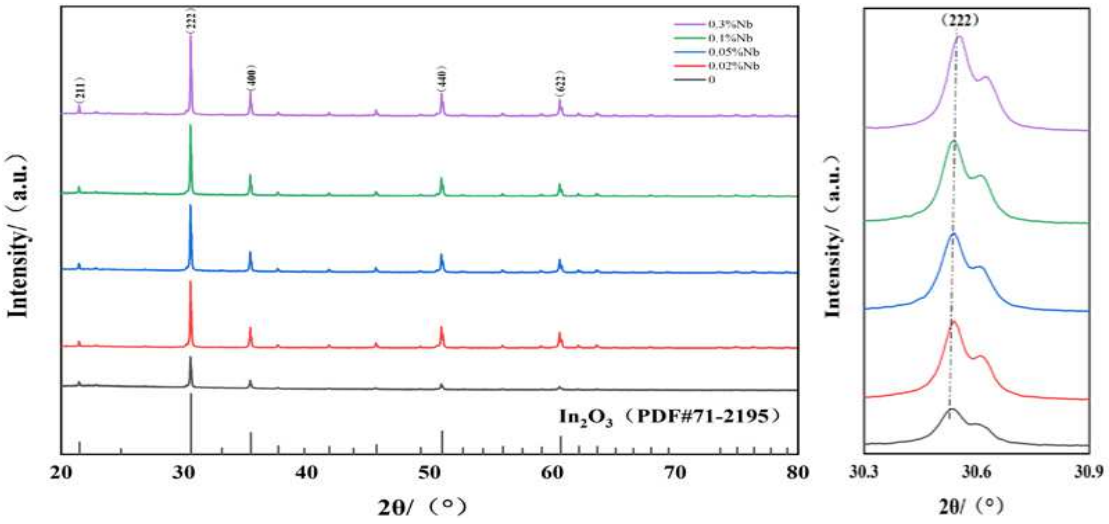


Fig. 2 XRD patterns of targets with different Nb_2O_5 contents sintered at 1450 °C for 6 h

Table 4 Comparison of Lattice Constants of ITO Targets

Lattice parameters / Sample Code	a(Å)	b(Å)	c(Å)
ITO-0	10.13395	10.13395	10.13395
ITO-1	10.12811	10.12811	10.12811
ITO-2	10.12900	10.12900	10.12900
ITO-3	10.12633	10.12633	10.12633
ITO-4	10.12690	10.12690	10.12690

Rw(ITO-0) = 5.160, Rw(ITO-1) = 7.660, Rw(ITO-2) = 6.164, Rw(ITO-3) = 6.443, Rw(ITO-4) = 7.431

Figure 3 presents the surface and cross-section micro-morphologies of ITO-0, ITO-1, ITO-2, ITO-3 and ITO-4 targets sintered at 1450 °C with a holding time of 6 h.

As observed from the surface micrographs, all ITO targets with different doping contents exhibit flat and smooth surfaces with distinct grain boundaries, negligible pores and uniform grain sizes. Transcrystalline fracture is identified for all samples from the cross-section observations, indicating high grain-boundary bonding strength and favorable densification of the sintered targets. Improved fracture toughness is achieved in terms of mechanical properties, so that cracking is less likely to occur during the cooling stage of sputtering deposition[30]. Obvious pores can be observed in the fracture morphologies shown in Figure 3(f), 3(g) and 3(h). Fewer pores are detected in Figure 3(g) and 3(h) compared with Figure 3(f), which is mainly ascribed to the sintering-aid effect exerted by doped Ti elements at this sintering temperature. The elimination of internal pores and highly dense fracture features are clearly seen in Figure 3(i), demonstrating an enhancement in the relative density of the target. A small number of micropores reappear inside the target in Figure 3(j), which corresponds to the degradation of relative density induced by excessive doping. It is demonstrated that appropriate addition of Nb_2O_5 dopant can also promote the sintering densification of ITO targets. By contrast, excessive doping introduces abundant point defects, by which the grain-boundary diffusion rate is increased remarkably. Rapid grain-boundary migration takes place during sintering, leaving residual pores inside the targets that can hardly be eliminated, and consequently the relative density is reduced[31].

Figure 4 presents the surface and cross-section micro-morphologies of ITO-3 targets sintered at 1400 °C, 1450 °C, 1500 °C, 1550 °C and 1600 °C, respectively. A small quantity of pores and insufficient grain growth can be observed in Figure 4(a). Figures 4(b) and 4(c) exhibit distinct grain boundaries and the absence of surface pores, revealing high surface densification. It indicates that the sintering-densification process of the targets is significantly accelerated with increasing sintering temperature, and grains are fully developed at this stage, which is beneficial for reducing grain-boundary scattering and improving carrier mobility. Figures 4(d) and 4(e) demonstrate that grain coarsening occurs on the surfaces of ITO-3 targets sintered at 1550 °C and 1600 °C. Grain coarsening causes internal pores to become detached from grain boundaries, whereby such pores are trapped within the target matrix and a slight decreasing trend in relative density is thereby produced[32]. The cross-section micrograph in Figure 4(f) reveals abundant internal pores in the target sintered at 1400 °C, as incomplete sintering is achieved and low relative density is obtained under this condition. No obvious internal pores are detected in Figures 4(g), 4(h), 4(i) and 4(j), and a high densification level is attained. Figure 5 shows the grain sizes of targets with different Nb_2O_5 wt% contents after sintering at 1450 °C for 6 h. According to the analysis of average grain sizes from Figure 5(a) to Figure 5(d), the average grain size is continuously decreased from 2.02 μm for the undoped sample to 1.76 μm. It suggests that appropriate Ti and

Nb additions can suppress grain growth of the targets at 1450 °C. As shown in Figure 5(e), the average grain size of ITO-4 target reaches 1.99 μm. This phenomenon indicates that the increased point defects introduced by excessive Nb doping bring about an elevated grain-boundary migration rate, and consequently only a minor difference in grain size is found between ITO-4 and ITO-0.

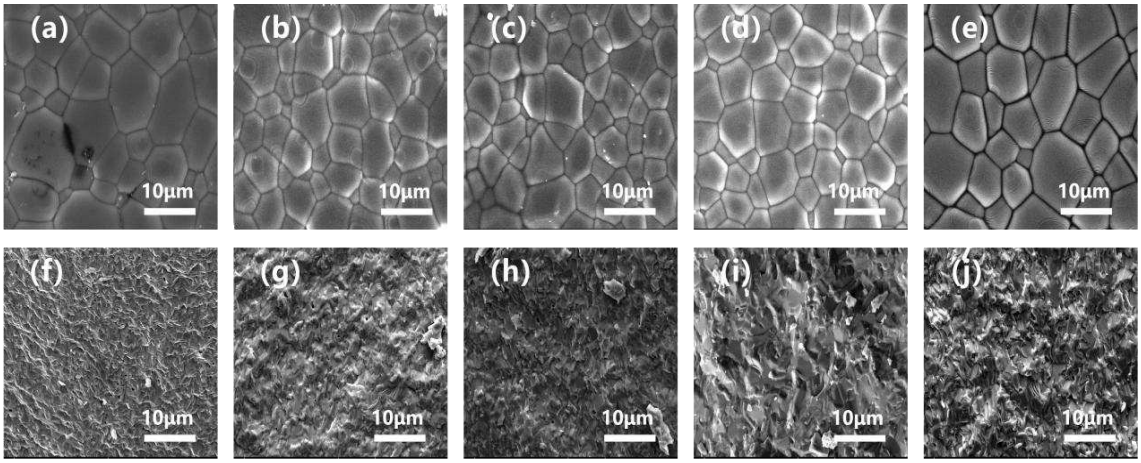


Fig. 3 SEM surface and cross-section images of targets with different Nb_2O_5 contents sintered at 1450 °C for 6 h

Surface: (a) ITO-0; (b) ITO-1; (c) ITO-2; (d) ITO-3; (e) ITO-4

Cross-section: (f) ITO-0; (g) ITO-1; (h) ITO-2; (i) ITO-3; (j) ITO-4

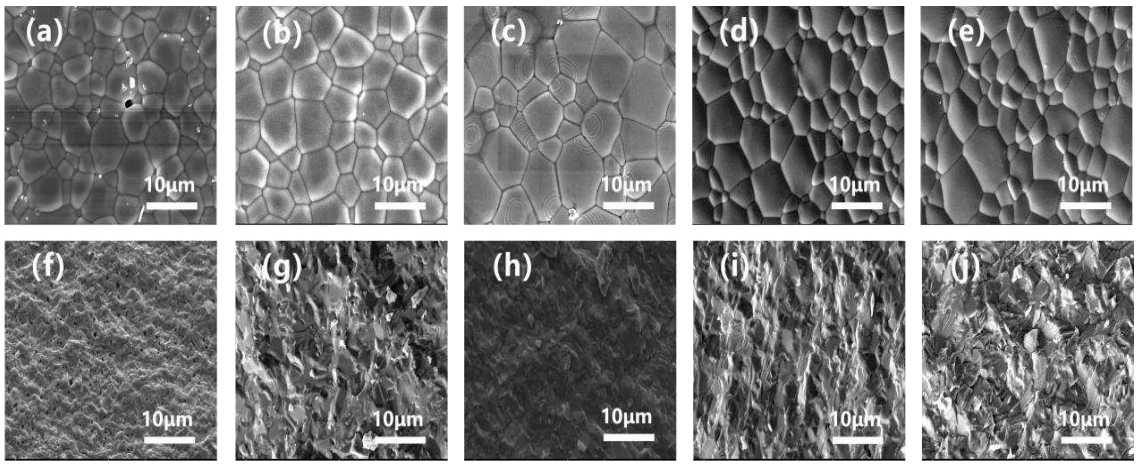


Fig. 4 SEM surface and cross-section images of ITO-3 targets sintered at different temperatures

Surface: (a) 1400 °C; (b) 1450 °C; (c) 1500 °C; (d) 1550 °C; (e) 1600 °C

Cross-section: (f) 1400 °C; (g) 1450 °C; (h) 1500 °C; (i) 1550 °C; (j) 1600 °C

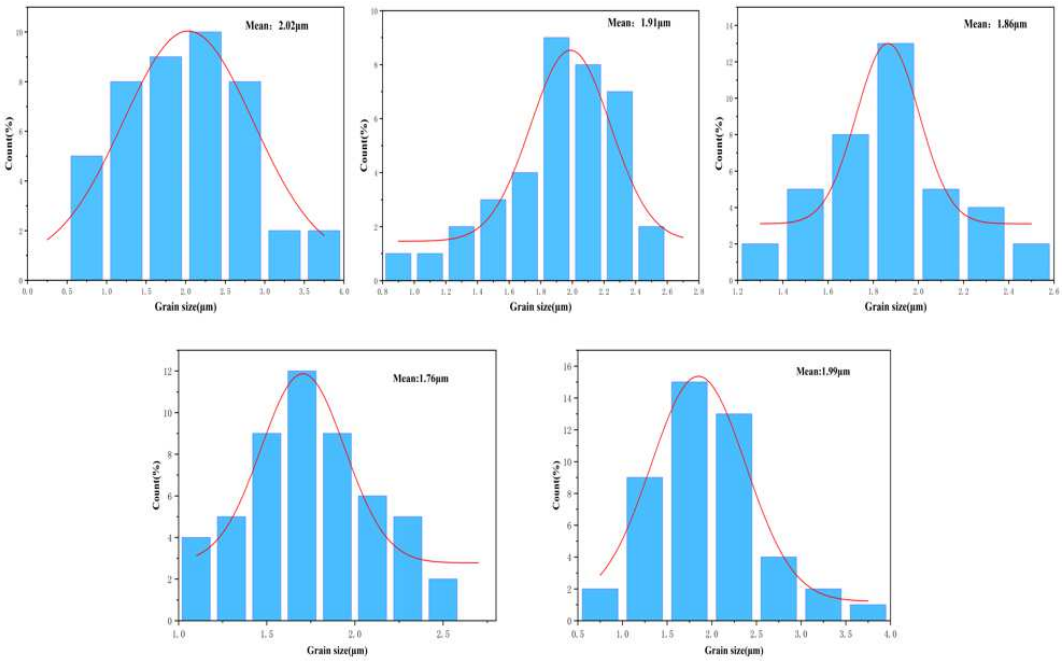


Fig. 5 Grain size distributions of ITO targets with different Nb_2O_5 contents sintered at 1450 °C for 6 h

(a) ITO-0; (b) ITO-1; (c) ITO-2; (d) ITO-3; (e) ITO-4

Figure 6 presents the elemental distribution of the ITO-3 target sintered at 1450 °C for 6 h. No discernible segregation of the four major elements is observed within the target. Such distribution characteristics are favorable for ITO sputtering deposition. During film-forming processes, homogeneous elemental distribution in the target can suppress the formation of nodular defects, yield uniform composition of the sputtered films and reduce defect gradients, which contributes to the improvement of film quality. Targets with uniform elemental distribution possess an extended service life. In the magnetron-sputtering process, comparable sputtering degrees are achieved over the entire target surface for homogeneously distributed targets. A complete etching morphology of the whole target is thereby obtained, which facilitates the enhancement of target utilization efficiency[33].

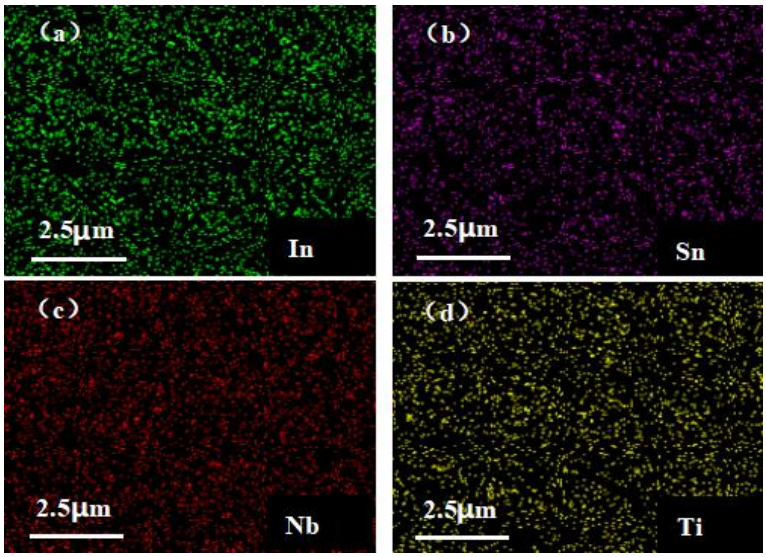


Fig. 6 EDS element distribution mappings of the ITO-3 target sintered at 1450 °C for 6 h

(a) In mapping; (b) Sn mapping; (c) Nb mapping; (d) Ti mapping

Figures 7(a) and 7(b) illustrate the variations in relative density and resistivity of targets with different Nb_2O_5 contents as a function of sintering temperature, respectively. As shown in Figure 7(a), the relative density of all targets is markedly improved within the temperature range from 1400 °C to 1450 °C, whereas the variation tendency of relative density slows down from 1450 °C to 1600 °C. This indicates that a sufficient driving force for densification is reached above 1450 °C for all targets. For doped targets, no further improvement in relative density is obtained when the sintering temperature is increased to 1500 °C; instead, a decline in relative density is observed. A recovery in relative density occurs upon further heating to 1550 °C, which is closely associated with the grain-boundary pinning effect induced by Nb-Ti elements. When the temperature is elevated to 1600 °C, the relative density of all targets is reduced. At this temperature, grain coarsening readily takes place within the targets, leading to a reduced elimination rate of generated pores. Meanwhile, the decomposition rates of SnO_2 and In_2O_3 are accelerated, giving rise to frequent pore formation and consequently a small number of residual internal pores. The maximum relative density of 99.54 % is achieved for the ITO-3 target at 1450 °C, while the relative density of ITO-0 only reaches 99.09 % under the identical condition. This demonstrates that appropriate Ti and Nb co-doping promotes the sintering densification of ITO targets. The formula for target resistivity is given as follows:

$$\rho = \frac{1}{ne\mu} \qquad (2)$$

In Equation (2), ρ denotes the resistivity, n represents the carrier concentration, μ stands for the carrier mobility, and e is the absolute value of the electronic charge.

Figure 7(b) compares the resistivity of ITO targets with different Nb doping contents measured at various sintering temperatures. It can be seen from Figure 7(b)

that the undoped ITO-0 target achieves a minimum resistivity of 2.086×10^{-4} Ω·cm at 1550 °C.For doped ITO-2, ITO-3 and ITO-4 targets, the minimum resistivity is obtained at 1450 °C. Among them, theITO-3 target exhibits the lowest resistivity of 1.940×10^{-4} Ω·cm at 1450 °C compared with other targets sintered at the same temperature. This result may be attributed to the electrons supplied by appropriate Ti^{4+} and Nb^{5+} donors as well as the modulation of oxygen vacancies. Within this doping range, the positive effect originating from carrier concentration dominates over the adverse effects induced by impurity ion scattering and Coulomb scattering. The minimum resistivity of the ITO-3 target at 1450 °C is also closely related to its high relative density at this sintering temperature. If the target possesses low relative density and abundant pores, both carrier mobility and carrier concentration will be greatly reduced, leading to an increase in resistivity.

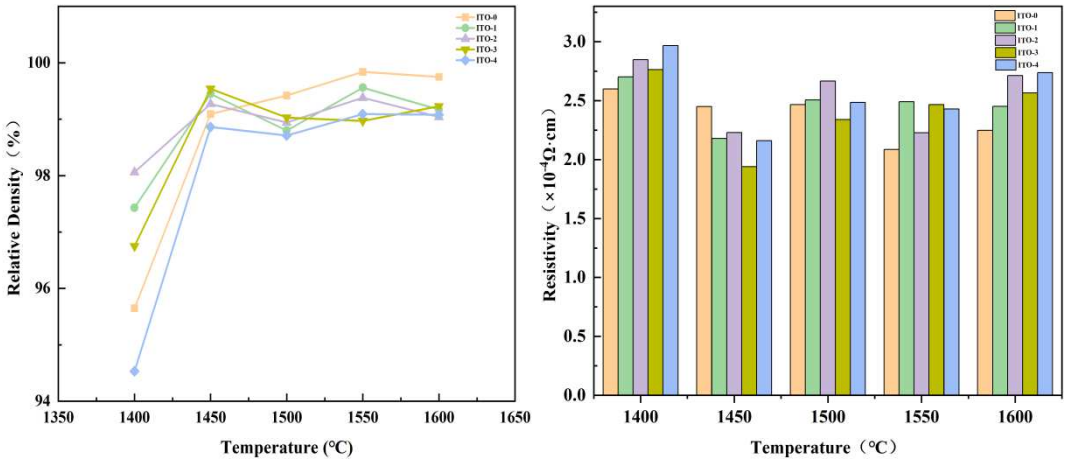


Fig. 7 (a) Relative density of targets with different Nb_2O_5 contents as a function of sintering temperature; (b) Resistivity of ITO targets with different Nb_2O_5 contents as a function of sintering temperature

Figure 8(a) reveals that the carrier mobility of the targets exhibits a non-monotonic variation: it first decreases, then increases, and finally declines with the rising Nb_2O_5 doping content. The carrier mobilities of ITO-0, ITO-1, ITO-2, ITO-3 and ITO-4 targets sintered at 1450 °C are 46.5, 41.7, 24.5, 57.4 and 28.2 $cm^2\cdot V^{-1}\cdot s^{-1}$, The carrier concentration of ITO-0, ITO-1, ITO-2, ITO-3 and ITO-4 targets sintered at 1450 °C are 5.48,6.02,11.5,5.6 and 10.2 $\times10^{20}$ cm^{-3},respectively. The reduction in mobility for targets with 0.02 wt% and 0.05 wt% Nb_2O_5 doping compared with the undoped sample originates from the incorporation of dopant ions into the host lattice. The aggravated lattice distortion strengthens lattice scattering gradually, and the ionized impurities introduced by doping enhance Coulomb scattering, which induces a remarkable drop in mobility. When the doping composition is 0.1 wt% Nb_2O_5–0.1 wt% TiO_2, the maximum carrier mobility is achieved for the target. It is speculated that partial compensation of lattice distortion triggered by dopant ions occurs at this doping level, whereby lattice scattering is alleviated. Meanwhile, the carrier concentration falls within an optimal range, generating the Coulomb screening effect to suppress ionized

impurity scattering to a certain extent. In addition, dopants are presumed to react with intrinsic oxygen vacancies in the host lattice. Consequently, the overall concentration of oxygen vacancies is reduced, the carrier trapping capability of oxygen vacancies is weakened, and the carrier mobility is improved[34]. Further increasing the doping content causes ionized impurity scattering to become dominant, and thereby the carrier mobility decreases substantially. As shown in Figure 8(b), the maximum mobility of the ITO-3 target is obtained at a sintering temperature of 1450 °C, and continuous elevation of sintering temperature leads to a persistent reduction in mobility. Increasing the temperature from 1400 °C to 1450 °C improves the relative density of the target and attenuates pore scattering, which contributes to the enhancement of carrier mobility. When the sintering temperature exceeds 1500 °C, the volatilization of In_2O_3 and SnO_2 is intensified at high temperatures, giving rise to more oxygen-vacancy defects， this results in a reduction in carrier mobility[35]. Moreover, some micropores reappear inside the target and strengthen pore scattering. Combined with ionized impurity scattering, this effect jointly restrains the improvement of carrier mobility.

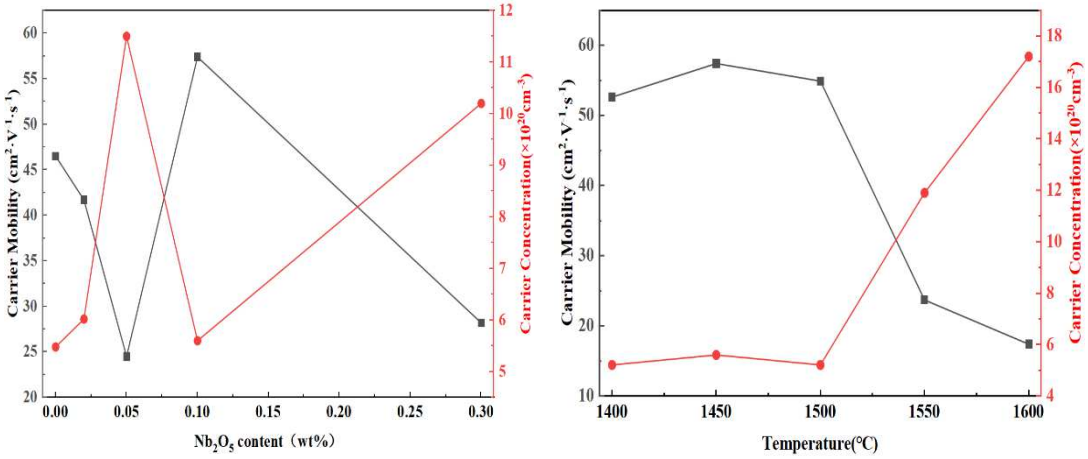


Fig. 8 (a) Carrier mobility and carrier concentration of samples with different Nb_2O_5 contents sintered at 1450 °C; (b) Carrier mobility and carrier concentration of the ITO-3 target at different sintering temperatures

4 Conclusions

This work mainly investigates the effects of Nb_2O_5–TiO_2 co-doping on the properties of ITO targets. It is found that co-doping with 0.1 wt% Nb_2O_5 and 0.1 wt% TiO_2 reduces the sintering temperature of ITO targets from 1550 °C to 1450 °C. The ITO-3 target sintered at 1450 °C for 6 h achieves a relative density of 99.54 %, a resistivity of 1.940×10^{-4} Ω·cm, and a carrier mobility of 57.4 $cm^2\cdot V^{-1}\cdot s^{-1}$. Appropriate co-doping of Nb_2O_5 and TiO_2 promotes densification, lowers the resistivity, and improves the carrier mobility of ITO targets. The underlying mechanism, involving the evolution of oxygen-vacancy concentration and the modulation of defect structures, requires further verification via oxygen vacancy characterization. The findings of this study can provide experimental

support for composition design and low-temperature sintering process optimization of co-doped ITO targets.

Funding Declaration

This work was financially supported by National Natural Science Foundation of China (Grant No. U21A2065, 62364007）;Guangxi Science and Technology Planning Project (Grant No. AD23023013, AA21077018);Guangxi Key R&D Program Project (Grant No. 2025FN96441017).

Acknowledgments

This work was financially supported by the National Natural Science Foundation of China (Grant Nos. U21A2065, 62364007), the Guangxi Science and Technology Planning Project (Grant Nos. AD23023013, AA21077018), and the Guangxi Key R&D Program Project (Grant No. 2025FN96441017). The authors appreciate all co-authors for their hard-working efforts and valuable contributions to this study. We also thank the testing platform of Guangxi Key Laboratory of Information Materials for its support in material characterizations.

References

[1] CHIANG Y C, SURYANTARI R, LIN S H. Electro-optic properties of liquid crystal cells with nanowall electrodes [J]. Opt Lett, 2023, 48(24): 6412–5.

[2] CAO M, WANG Q, SHANG J. Low-cost Sn-doped indium oxide films with high mobility by reactive plasma deposition for silicon heterojunction solar cells [J]. Solar Energy Materials and Solar Cells, 2024, 273: 112954.

[3] CHEN J, ZHONG J, LUO W. Study on powder preparation of IGZO target and its effect on sintering [J]. Journal of Alloys and Compounds, 2019, 800: 468–77.

[4] ZAKARIAE E-N, ALEXANDRE B, PERRINE C. High performance IWO thin films deposited with a new hybrid technology for solar cell applications [J]. Vacuum, 2025, 239: 114395.

[5] HAN B, SUN B, CHEN L. Tb doped IZO targets: Synergistic control of densification, microstructure, and electrical properties [J]. Ceramics International, 2025, 51(30): 62808–17.

[6] LEI P, CHEN X, YAN Y. Transparent and conductive IZO films: Oxygen and discharge voltage controlled sputtering growth and properties [J]. Vacuum, 2022, 195: 110645.

[7] XING Q, HUANG T, KONG D. Sintering densification behavior of nano-ITO powder with high oxygen vacancy induced via plasma stimulation [J]. Ceramics International, 2024, 50(13): 22922–35.

[8] KIM J G, LEE J E, JO S M. Room temperature processed high mobility W-doped In_2O_3 electrodes coated via in-line arc plasma ion plating for flexible OLEDs and quantum dots LEDs [J]. Sci Rep, 2018, 8(1): 12019.

[9] FAN C-L, TSAO H-Y, CHEN C-Y. New Low-Voltage Driving Compensating Pixel Circuit Based on High-Mobility Amorphous Indium-Zinc-Tin-Oxide Thin-Film Transistors for High-Resolution Portable Active-Matrix OLED Displays [J]. Coatings, 2020, 10(10): 1004.

[10] MEI F, QIN K, YUAN T. Effects of oxygen flow velocity on the sintering properties of ITO targets [J]. Journal of Materials Science: Materials in Electronics, 2017, 28(19): 14711–9.

[11] JUANG F-S, CHEN J-Y, KUO W-K. The Improvement of Luminous Uniformity of Large-Area Organic Light-Emitting Diodes by Using Auxiliary Electrodes [J]. Photonics, 2024, 11(9): 829.

[12] ZHANG Z, YU X, ZHAO W. Preparation of Low-Resistance and Residue-free ITO Films for Large-scale 3D Displays [J]. ACS Applied Materials & Interfaces, 2019, 11(49): 45903–13.

[13] FANG Y, REN Y, SONG Y. Benzoylacetone-induced (400) facet preference in ITO films and its enhancement on conductive properties [J]. Ceramics International, 2026, 52(6): 7054–62.

[14] ZHAO B, ZHU Y, XU Y. Efficient p-i-n-p blue OLED devices by inserting organic heterojunctions for charge generation [J]. Displays, 2025, 87: 102959.

[15] EGBO K O, ADESINA A E, EZEH C V. Effects of free carriers on the optical properties of high mobility transition metal doped In_2O_3 transparent conductors [J]. Physical Review Materials, 2021, 5(9): 094603.

[16] SUSAROVA D K, AKKURATOV A V, KUKHARENKO A I. ITO Modification for Efficient Inverted Organic Solar Cells [J]. Langmuir, 2017, 33(39): 10118–24.

[17] M.MURAOKA, M.SUZUKI, Y.SAWADA. Sintering of tin-doped indium oxide (Indium-Tin-Oxide, ITO) with Bi_2O_3 additive [J]. Journal of Materials Science, 1998, 33: 5621–4.

[18] M.SUZUKI, M.MURAOKA, Y.SAWADA. Sintering of indium–tin–oxide with vanadium oxide additive [J]. Materials Science and Engineering, 1998, B(54): 46–50.

[19] CHEN D, JIANG C, SUN H. Sintering study of ITO using a ZnO-doped and microwave hybrid sintering approach [J]. Journal of Asian Ceramic Societies, 2018, 2(1): 58–63.

[20] HUANG J, YUAN T, MEI F. Effects of cerium oxide doping on the microstructure and properties of ITO targets and the photoelectric properties of the films [J]. Journal of Materials Science: Materials in Electronics, 2019, 30(16): 15469–81.

[21] LIANG F, LIU J. Sintering, microstructure and electricity properties of ITO targets with Bi_2O_3 –Nb_2O_5 addition [J]. Ceramics International, 2017, 43(8): 5856–61.

[22] ZHAI X, ZHANG X, MA Y. Influence of Bi_2O_3-TiO_2 Additives and Sintering Process on the Performance of ITO Target Based on Normal Pressure Sintering Method [J]. Transactions of the Indian Ceramic Society, 2019, 78(2): 83–8.

[23] LIU T, JIANG Z, LIU J. Achieving high relative density and low resistivity in indium tin oxide targets via Bi_2O_3-CeO_2 additive [J]. Journal of Alloys and Compounds, 2023, 968: 171998.

[24] GE C, ER X, XIE X. Enhanced electrical conductivity of Zr-doped indium oxide-based targets via GeO_2-TiO_2 additive [J]. Materials Research Bulletin, 2026, 201: 114111.

[25] WANG T, XU J, ZHU G. Sintering densification of ITO targets with low tin oxide content for depositing TCO films as electrodes of solar cells [J]. Ceramics International, 2024, 50(3): 5532–40.

[26] YAO Z, DUAN W, STEUTER P. Influence of Oxygen on Sputtered Titanium-Doped Indium Oxide Thin Films and Their Application in Silicon Heterojunction Solar Cells [J]. Solar RRL, 2021, 5(1): 2000501.

[27] MEI F, YUAN T, LI R. Effects of particle size and dispersion methods of In_2O_3-SnO_2 mixed powders on the sintering properties of indium tin oxide ceramics [J]. International Journal of Applied Ceramic Technology, 2018, 15(1): 89–100.

[28] XIONG T, FENG B, ZHANG H. The Effect of Nb Doping on the Thermoelectric Properties of Indium Oxide [J]. Inorganics, 2025, 13(11): 356.

[29] ZHONG W, ZENG J, ZHOU X. Regulation of oxygen vacancies in ITO powders and its impact on densification behavior [J]. Journal of the European Ceramic Society, 2025: 117829.

[30] MILMAN Y V, CHUGUNOVA S. Mechanical properties, indentation and dynamic yield stress of ceramic targets [J]. International journal of impact engineering, 1999, 23(1): 629–38.

[31] LI X, LIU C, SUN B. Refined grain size of ITO ceramic targets prepared by pressure slip casting and two-step sintering [J]. Journal of the European Ceramic Society, 2021, 41(6): 3501–11.

[32] ZHANG J, LUDWIG W, ZHANG Y. Grain boundary mobilities in polycrystals [J]. Acta Materialia, 2020, 191: 211–20.

[33] MEI F, YUAN T, LI R. Effects of second-phase particles and elemental distributions of ITO targets on the properties of deposited ITO films [J]. Ceramics International, 2017, 43(12): 8866–72.

[34] OMATA T, FUJIWARA H, OTSUKA-YAO-MATSUO S. Electron trapping center and SnO2-doping mechanism of indium tin oxide [J]. Applied Physics A, 2000, 71(6): 609–14.

[35] GE C, LIU Z, ZHU Y. Insight into the high mobility and stability of In2O3: H film [J]. Small, 2024, 20(2): 2304721.